Coupled Systems Mechanics, *Vol. 12, No. 4 (2023) 391-407*
https://doi.org/10.12989/csm.2023.12.4.391

Effect of shear stresses on the deflection and optimal configuration of a rectangular FGM structure

Ayoub El Amrani[1a], Hafid Mataich[1b], Jaouad El-Mekkaoui[2c] and Bouchta El Amrani*[1]

[1]*Laboratory of Mathematics, Modeling and Applied Physics, High Normal School, Sidi Mohamed Ben Abbellah University, 30040 Fez, Morocco*
[2]*Laboratory of Technology and Innovations, High School of Technology, Sidi Mohamed Ben Abbellah University, 30040 Fez, Morocco*

(Received Novemer 8, 2022, Revised August 20, 2023, Accepted September 4, 2023)

Abstract. This paper presents a static study of a rectangular functional graded material (FGM) plate, simply supported on its four edges, adopting a refined higher order theory that looks for, only, four unknowns, without taking into account any corrective factor of the deformation energy with the satisfaction of the zero shear stress conditions on the upper and lower faces of the plate. We will have determined the contribution of these stresses in the transverse deflection of the plate, as well as their effects on the axial stress within the interfaces between the layers (to avoid any problem of imperfections such as delamination) and on the top and bottom edges of the plate in order to take into account the fatigue phenomenon when choosing the distribution law of the properties used during the design of the plate. A numerical statement, in percentage, of the contribution of the shear effect is made in order to show the reliability of the adopted theory. We will also have demonstrated the need to add the shear effect when the aspect ratio is small or large. Code routines are programmed to obtain numerical results illustrating the validity of the model proposed in the theory compared to those available in the literature.

Keywords: deflection; FGM; form function; refined higher order theory; shear stress

1. Introduction

Composite materials have the ability to combine thermal and mechanical properties within the same structure, but from the first composite parts tested, local optimization problems of these properties reside at the interfaces between layers, so to overcome the constraint of abrupt change in composition between layers of the structure, researchers in modern technology develops new materials, the functional graded material (FGM), further information can see Mahamood and Akinlabi (2017), Garg *et al.* (2020).

FGMs are considered composites at the microscopic scale whose properties may be considered

*Corresponding author, Ph.D., E-mail: bouchta.elamrani@usmba.ac.ma
[a]Ph.D., E-mail: elamrani.ay@gmail.com
[b]Ph.D., E-mail: hafid.mataich@usmba.ac.ma
[c]Ph.D., E-mail: jaouad.elmekkaoui@usmba.ac.ma

http://www.techno-press.org/?journal=csm&subpage=8 ISSN: 2234-2184 (Print), 2234-2192 (Online)

inhomogeneous, but at the macroscopic scale the change in volume fraction continuously in the desired direction, to have a tendency to reduce the stress concentration at the transition between adjacent layers and also reduces the residual and thermal stresses, making this type of structures as homogeneous as it is presented in Jin and Batra (1996), Abdelbaki *et al.* (2022), Liu *et al.* (2023), Rizov (2021). FGMs have a very crucial role when it comes to civil and aerospace structures that are subjected to operating conditions where the temperature is very high.

In our present study we deal with a type of FGM based on a metal (Aluminium, Al) and a ceramic (Alumina, Al_2O_3) it is the mixture that satisfies the needs for some applications where the metal transmits the property of toughness to the structure and the ceramic constituent gives high thermal resistance, Rabboh *et al.* (2013), Arslan and Gunes (2018).

To have a response (static or dynamic) of a loaded mechanical structure, we can base on theoretical methods like Navier techniques, a review is presented by Reddy (1984), Aghababaei and Reddy (2009) , Bekki *et al.* (2021), Bouhlali *et al.* (2019), these techniques are used when the boundary conditions are simply supported, on the other hand Levy's methods, the reader can read Bai and Chen (2012), Thai and Kim (2012), these methods have the ability to solve cases where two of the edges are simply supported regardless of the others. If the geometry is complicated, varied boundary conditions or loads that have random behavior, one should consider using numerical methods such as finite elements, Swaminathan and Patil (2008), Rao and Desai (2004), Sadeghi (2021), Singh and Harsha (2020), Sahoo *et al.* (2022) examined a finite element based method during the analysis of composite plates and FGM, similarly for Rayleigh-Ritz method as presented in the work of Fazzolari and Carrera (2014), Kumar and Lal (2012) or others.

The analysis of rectangular structures based on functional gradient materials, FGM, relies on three groups of theories, depending on the geometry of the plates and the desired accuracy of the results, firstly, the classical plate theory (CPT) which is the easiest to handle is that for its neglect of the shear effects as it presented in Javaheri and Eslami (2002), Najafizadeh, Hedayati (2004), this theory is inaccurate for thick geometry, which pushed the research towards other analysis methods such as first order shear deformation theory (FSDT) and that to take into account the shear effects to analyze thin and medium thick plates, in this context, Nguyen-Xuan *et al.* (2011), Nguyen-Xuan *et al.* (2012), Karakoti *et al.* (2022) have presented examples of the use of FSDT, but the accuracy of the results obtained is strongly related to the correct choice of the shear stress correction factor in order to regularize the contribution of the shear strain energy in the analysis. To overcome the limitations and drawbacks of the previous theories we increase the order of development of the displacement field, the higher order models, Bhaskar *et al.* (2021), Taczala *et al.* (2022), Kablia *et al.* (2022), Soelarso *et al.* (2021), include higher order approximations of the displacement field give more accurate results than the previous approximations. As well as other refined theory have been developed, particularly, the sinusoidal shear deformation theory (SSDT) as presented by Zenkour (2006), Liang and Wang (2020) and the hyperbolic shear deformation theory (HSDT), an example was presented by Benyoucef *et al.* (2010), Youcef *et al.* (2020), Belkhodja *et al.* (2023).

The present study uses a refined higher order theory that uses only four variables to completely determine the displacement field (u_x, u_y, u_z) of any point (x, y, z) of the FGM plate, $\Omega x(h/2\,, -h/2)$.

The refined theory adopted respects the nullity of shear stresses at the upper and lower interfaces of the plate through a proposed shape function $f(z)$ see Table 2.

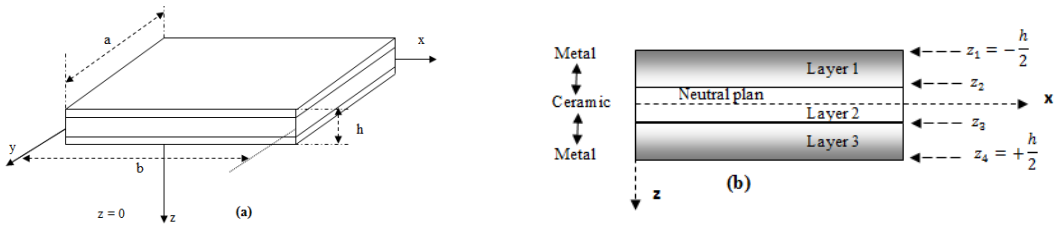

(a) Geometric properties (b)Material properties

Fig. 1 Geometric properties and material properties of the rectangular structure (FGM)

Table 1 Properties of the materials used in the studied plate

Properties	Aluminium, Al	Alumina, Al_2O_3
Young's modulus	$E_m = 70.0$ MPa	$E_c = 380.0$ MPa
Poisson's ratio	$\nu = 0.3$	$\nu = 0.3$

2. Presentation of the problem studied

In this paper we want to make a numerical study to have the effect of transverse shear stresses on the deflection as well as the optimal configurations of a rectangular structure with gradually changing material properties (FGM plate).

2.1 Geometric properties of the plates

In this study we treat a sandwich plate of rectangular shape composed of three layers of width a and length b with uniform thickness h, loaded under a mechanical load $q(x, y)$ in the Cartesian coordinate system (x, y, z) whose surface $z = 0$ coinciding with the neutral surface of the plate, as shown in Fig. 1(a).

The ordinates z_k in the direction of positive *z*, the different ordinates limits of the three layers are, $z_1 = -h/2\,, z_2, z_3$ and $z_4 = +h/2$ see Fig. 1(b).

The studied three-layer plates are presented with diagrams [e-f-g], the three numbers *e*, *f* and *g* represent the ratio between the layer thickness h_k and the global thickness *h*.

Remarks

◦ In MATLAB we use $z_1 = -h/2$ and $z_{k+1} = z_k + h_k$ with $k \in \{1,2,3,4,\dots\}$ which represents the layer number and h_k their thickness.

◦ In MATLAB we use $h_1 = e\,h/S\,,\ h_2 = f\,h/S$ and $h_3 = g\,h/S$, with $S = e + f + g$

2.2 Properties of the materials Al_2O_3 and Al

The mechanical and thermal properties of the two materials used are presented in Table 1.

The central layer is entirely made of ceramic while layers 1 and 2 are made of a mixture (FGM) of the two materials aluminum Al and ceramic Al_2O_3 combined together according to a power law, whose volume fraction through the *z*-order is presented as follows

$$V_c^{(1)} = \left(\frac{z - z_1}{z_2 - z_1}\right)^p, z \in [z_1, z_2] \qquad V_c^{(2)} = 1\ , z \in [z_2, z_3] \qquad V_c^{(3)} = \left(\frac{z - z_4}{z_3 - z_4}\right)^p, z \in [z_3, z_4] \quad (1)$$

$$\text{With } V_m^{(k)} = 1 - V_c^{(k)}$$

The volume fractions of ceramic and aluminum are respectively for the *k* layer, $V_c^{(k)}$ and $V_m^{(k)}$ and p indicates the index of the power law used such as $(p \geq 0)$ depending on the desired optimization of the properties through the thickness.

The material properties of an FGM configuration that varies only through the thickness *h* are calculated following the rule of Mori and Tanaka (1973).

$$P^{(k)}(z) = V_c^{(k)}(z).P_c + \left[1 - V_c^{(k)}(z)\right].P_m \tag{2}$$

$P^{(k)}(z)$ is the effective property of the *k*-layer at a point *z* regardless of *x* and *y* in Ω.

Example: for the Young's modulus of a layer *k* of the Al/Al_2O_3 plate, with E_m, E_c the Young's modulus of aluminium and ceramic respectively.

$$E^{(k)}(z) = V_c^{(k)}(z).E_c + \left[1 - V_c^{(k)}(z)\right].E_m \tag{3}$$

The curves in Fig. 2 show the variation of Young's modulus $E(z)$ through the thickness h of the FGM plate for the three layers and three values of the index $p \in \{0.05,1,10\}$.

N.B.: In this study, it is assumed that the Poisson's ratio is constant $\nu = Cst, \forall\, z$.

3. Theory adopted and mathematical formulation of the problem

3.1 Assumptions

• To have infinitesimal deformations we consider that the thickness h of the plate is very large compared to the displacements

• Displacements due to extension effects $u_{x0}(x,y)$ - $u_{y0}(x,y)$ of flexion $u_x^b(x,y)$ - $u_y^b(x,y)$ and shear effects $u_x^s(x,y)$ - $u_y^s(x,y)$ are accumulated to have the displacements $u_x(x,y,z)$, $u_y(x,y,z)$ in the *x* and *y* directions respectively, then

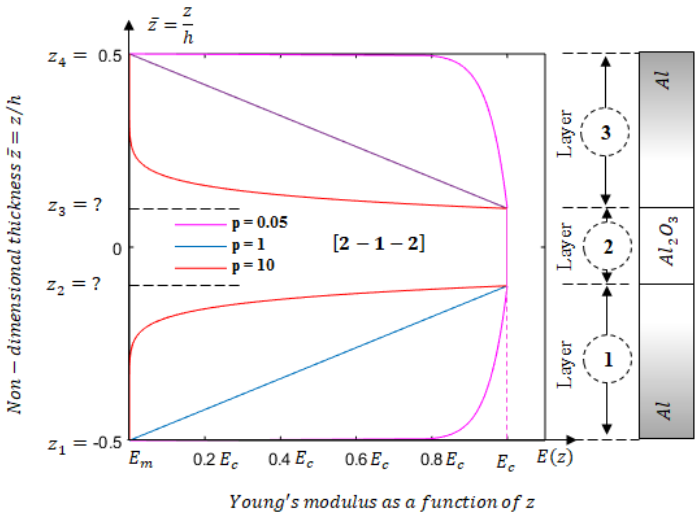

Fig. 2 Variation of Young's modulus of the three-layer FGM plate

Table 2 Proposed model for the shape function $f(z)$

Proposed model	Form function $f(z)$	$f'(z) = df(z)/dz$
Proposed model 1	$(h/\pi)\sin(\sin(\pi z/h))$	$\cos(\pi z/h)\cos(\sin(\pi z/h))$
Proposed model 2	$(h/\pi)\tanh(\sin(\pi z/h))$	$\cos(\pi z/h)(1-(\tanh(\sin(\pi z/h)))^2)$
Model Arya *et al.*	$(h/\pi)\sin((\pi z/h))$	$\cos(\pi z/h)$
Model Karama *et al.*	$z(\exp(-2(z/h)^2))$	$(1-(4z^2/h^2))\,exp(-2(z/h)^2)$
Reddy model	$z-(4/3)(z^3/h^2)$	$1-(4z^2/h^2)$

$$u_x(x,y,z) = u_{x0}(x,y) + u_x^b(x,y) + u_x^s(x,y),$$
$$u_y(x,y,z) = u_{y0}(x,y) + u_y^b(x,y) + u_y^s(x,y) \quad (4)$$

• Taking into account the transverse shear displacements, the global deflection $u_z(x,y,z)$ contains two components u_{z0}^s, u_{z0}^b due to shear and bending respectively, as

$$u_z(x,y,z) = u_{z0}^b(x,y) + u_{z0}^s(x,y) \quad (5)$$

• The axial stress along the z axis, σ_z is very small compared to those σ_x and σ_y so we can neglect it.

As the classical plate approach we will note

$$u_x^b(x,y) = -z\,\partial\, u_{z0}^b/\partial x \text{ and } u_y^b(x,y) = -z\,\partial\, u_{z0}^b/\partial y \quad (6)$$

Travel $u_x^s(x,y)$ and $u_y^s(x,y)$ deformations are derived γ_{xz} and γ_{yz} which vary parabolically through the thickness h, all respecting the condition of cancelling the transverse stresses τ_{xz} and τ_{yz} on both sides of the plate.

$$u_x^s(x,y) = -f(z)\,\partial\, u_{z0}^s/\partial x \text{ and } u_y^s(x,y) = -f(z)\,\partial\, u_{z0}^s/\partial y \quad (7)$$

The parabolic variation of the strains and the nullity of the transverse stresses on the two faces of the plate is ensured by proposals of two shape functions $f(z)$ and to validate them we use models in the literature, Arya *et al.* (2002), Karama *et al.* (2003), Reddy (2000).

The first comparison of our proposed models (1 and 2) with the literature is made in Fig. 6, are models that respect the parabolic variation through the thickness and also the nullity of transverse stresses on both the top and bottom faces of the plate.

3.2 Geometric equations, deformation-displacement

Based on the last three assumptions in the previous section, the displacement field of the refined theory adopted in this study is as follows

$$\begin{Bmatrix} u_x(x,y,z) \\ u_y(x,y,z) \\ u_z(x,y,z) \end{Bmatrix} = \begin{Bmatrix} u_{x0}(x,y) - z\frac{\partial u_{z0}^b(x,y)}{\partial x} - f(z)\frac{\partial u_{z0}^s(x,y)}{\partial x} \\ u_{y0}(x,y) - z\frac{\partial u_{z0}^b(x,y)}{\partial y} - f(z)\frac{\partial u_{z0}^s(x,y)}{\partial y} \\ u_{z0}^b(x,y) + u_{z0}^s(x,y) \end{Bmatrix} \quad (8)$$

With $u_x(x,y,z)$, $u_y(x,y,z)$, $u_z(x,y,z)$ are the elements of the displacement field according to the theory used.

We neglect the Von Karman or more deformation terms, the linear deformation field is written for the k layer as follows

$$\begin{Bmatrix}\varepsilon_x\\ \varepsilon_y\\ \gamma_{xy}\\ \gamma_{yz}\\ \gamma_{xz}\end{Bmatrix}^{(k)} = \begin{Bmatrix}\frac{\partial u_{x0}}{\partial x} - z\frac{\partial^2 u_{z0}^b}{\partial x^2} - f(z)\frac{\partial^2 u_{z0}^s}{\partial x^2}\\ \frac{\partial u_{y0}}{\partial x} - z\frac{\partial^2 u_{z0}^b}{\partial y^2} - f(z)\frac{\partial^2 u_{z0}^s}{\partial y^2}\\ \frac{\partial u_{x0}}{\partial y} + \frac{\partial u_{y0}}{\partial x} - 2z\frac{\partial^2 u_{z0}^b}{\partial x\partial y} - 2f(z)\frac{\partial^2 u_{z0}^s}{\partial x\partial y}\\ \left(1-\frac{\partial f}{\partial z}\right)\frac{\partial u_{z0}^s}{\partial y}\\ \left(1-\frac{\partial f}{\partial z}\right)\frac{\partial u_{z0}^s}{\partial x}\end{Bmatrix}^{(k)} = \begin{Bmatrix}\varepsilon_x^0 + z\chi_x^b + f(z)\chi_x^s\\ \varepsilon_y^0 + z\chi_y^b + f(z)\chi_y^s\\ \gamma_{xy}^0 + z\chi_{xy}^b + f(z)\chi_{xy}^s\\ \left(1-\frac{\partial f}{\partial z}\right)\gamma_{yz}^s\\ \left(1-\frac{\partial f}{\partial z}\right)\gamma_{xz}^s\end{Bmatrix}^{(k)} \quad (9)$$

With $\varepsilon_x, \varepsilon_y, \gamma_{xy}, \gamma_{yz}\ et\ \gamma_{xz}$ the elements of the deformation field.

3.3 Constitutive equations, stress-strain

We apply Hooke's law for our case of a linear elastic and orthotropic FGM plate, with the assumption $\sigma_z = 0$. According to the fourth assumption, then for each layer *k*, the stress field is

$$\begin{Bmatrix}\sigma_x\\ \sigma_y\\ \tau_{xy}\end{Bmatrix}^{(k)} = \begin{bmatrix}Q_{11}(z) & Q_{12}(z) & 0\\ Q_{12}(z) & Q_{22}(z) & 0\\ 0 & 0 & Q_{66}(z)\end{bmatrix}^{(k)} \begin{Bmatrix}\varepsilon_x\\ \varepsilon_y\\ \gamma_{xy}\end{Bmatrix}^{(k)}$$
$$\text{and } \begin{Bmatrix}\tau_{yz}\\ \tau_{xz}\end{Bmatrix}^{(k)} = \begin{bmatrix}Q_{44}(z) & 0\\ 0 & Q_{55}(z)\end{bmatrix}^{(k)} \begin{Bmatrix}\gamma_{yz}\\ \gamma_{xz}\end{Bmatrix}^{(k)} \quad (10)$$

With $\sigma_x, \sigma_y, \tau_{xy}, \tau_{yz}$ and τ_{xz} the elements of the stress field.

The use of the relation (3) allows us to calculate the stiffnesses of the material as a function of the order *z* for each layer "*k*".

$$Q_{11}^{(k)}(z) = Q_{22}^{(k)}(z) = \frac{E(z)}{1-v^2},\ Q_{12}^{(k)}(z) = \frac{vE(z)}{1-v^2}\ ;\ Q_{44}^{(k)}(z) = Q_{55}^{(k)} = Q_{66}^{(k)} = \frac{E(z)}{2(1+v)}$$
$$\text{and } Q_{16}^{(k)} = Q_{26}^{(k)} = 0 \quad (11)$$

3.4 Governing equations of motion

The principle of virtual work applied in the static case allows us to obtain the governing equations of motion:

$$\forall\ \delta u_{x0} : \frac{\partial N_x}{\partial x} + \frac{\partial N_{xy}}{\partial y} = 0$$
$$\forall\ \delta u_{y0} : \frac{\partial N_{xy}}{\partial x} + \frac{\partial N_y}{\partial y} = 0$$
$$\forall\ \delta u_{z0}^b : \frac{\partial^2 M_x^b}{\partial x^2} + 2\frac{\partial^2 M_{xy}^b}{\partial x\partial y} + \frac{\partial^2 M_y^b}{\partial y^2} + q = 0$$
$$\forall\ \delta u_{z0}^s : \frac{\partial^2 M_x^s}{\partial x^2} + 2\frac{\partial^2 M_{xy}^s}{\partial x\partial y} + \frac{\partial^2 M_y^s}{\partial y^2} + \frac{\partial S_{xz}^s}{\partial x} + \frac{\partial S_{yz}^s}{\partial y} + q = 0 \quad (12)$$

Geometrically we can write:

$$\begin{bmatrix} N_x & N_y & N_{xy} \\ M_x^b & M_y^b & M_{xy}^b \\ M_x^s & M_y^s & M_{xy}^s \end{bmatrix} = \sum_{k=1}^{3} \left(\int_{z_k}^{z_{k+1}} \begin{Bmatrix} 1 \\ z \\ f(z) \end{Bmatrix} (\sigma_x, \sigma_y, \tau_{xy})^{(k)} \, dz \right).$$

$$\begin{Bmatrix} S_{yz}^s \\ S_{xy}^s \end{Bmatrix} = \sum_{k=1}^{3} \left(\int_{z_k}^{z_{k+1}} (1 - \frac{df(z)}{dz}) \begin{Bmatrix} \tau_{yz} \\ \tau_{xz} \end{Bmatrix}^{(k)} dz \right) \quad (13)$$

If we integrate these formulas through the thickness we obtain the following stiffnesses (main and coupling)

$$\begin{Bmatrix} N \\ M^b \\ M^s \end{Bmatrix} = \sum_{k=1}^{n} \begin{bmatrix} [\mathrm{A}] & [\mathrm{B}] & [B^s] \\ [\mathrm{B}] & [\mathrm{D}] & [D^s] \\ [B^s] & [D^s] & [H^s] \end{bmatrix}^{(k)} \begin{Bmatrix} \varepsilon \\ \kappa^b \\ \kappa^s \end{Bmatrix} \; et \; \begin{Bmatrix} S_{yz}^s \\ S_{xz}^s \end{Bmatrix} = \sum_{k=1}^{n} \begin{bmatrix} A_{44}^s & 0 \\ 0 & A_{55}^s \end{bmatrix}^{(k)} \begin{Bmatrix} \gamma_{yz}^s \\ \gamma_{xz}^s \end{Bmatrix} \quad (14)$$

Where A_{ij}, B_{ij} ... etc, are the rigidities of the plate.

Substituting expressions (14) into Eq. (12) gives us the system of equations in terms of the operators applied to the searched displacement field, as

$$[O]\{\delta\} = \{f\} \Longrightarrow \begin{bmatrix} O_{11} & O_{12} & O_{13} & O_{14} \\ O_{12} & O_{22} & O_{23} & O_{24} \\ O_{13} & O_{23} & O_{33} & O_{34} \\ O_{14} & O_{24} & O_{34} & O_{44} \end{bmatrix} \begin{Bmatrix} u_{x0} \\ u_{y0} \\ u_{z0}^b \\ u_{z0}^s \end{Bmatrix} = \begin{Bmatrix} 0 \\ 0 \\ q(x,y) \\ \mathrm{q(x,y)} \end{Bmatrix} \quad (15)$$

Where, $\{\delta\} = \{u_{x0}, u_{y0}, u_{z0}^b, u_{z0}^s\}^T$ is the vector of displacements of a point (x, y) of the median plane and $\{f\} = \{0,0,q(x,y),q(x,y)\}^T$ the vector of generalized forces, with $[O]$ the symmetric matrix of differential operators such that

$$O_{11} = A_{11}\frac{\partial^2}{\partial x^2} + A_{66}\frac{\partial^2}{\partial y^2}. \qquad O_{12} = (A_{12} + A_{66})\frac{\partial^2}{\partial x \partial y}.$$

$$O_{13} = -B_{11}\frac{\partial^3}{\partial x^3} - (B_{12} + 2B_{66})\frac{\partial^3}{\partial x \partial y^2}. \qquad O_{14} = -B_{11}^s\frac{\partial^3}{\partial x^3} - (B_{12}^s + 2B_{66}^s)\frac{\partial^3}{\partial x \partial y^2}.$$

$$O_{22} = A_{66}\frac{\partial^2}{\partial x^2} + A_{22}\frac{\partial^2}{\partial y^2}. \qquad O_{23} = -B_{22}\frac{\partial^3}{\partial y^3} - (B_{12} + 2B_{66})\frac{\partial^3}{\partial x^2 \partial y}.$$

$$O_{24} = -B_{22}^s\frac{\partial^3}{\partial y^3} - (B_{12}^s + 2B_{66}^s)\frac{\partial^3}{\partial x^2 \partial y}. \qquad O_{33} = D_{11}\frac{\partial^4}{\partial x^4} + 2(D_{12} + 2D_{66})\frac{\partial^4}{\partial x^2 \partial y^2} + D_{22}\frac{\partial^4}{\partial y^4}.$$

$$O_{34} = D_{11}^s\frac{\partial^4}{\partial x^4} + 2(D_{12}^s + 2D_{66}^s)\frac{\partial^4}{\partial x^2 \partial y^2} + D_{22}^s\frac{\partial^4}{\partial y^4}.$$

$$O_{44} = H_{11}^s\frac{\partial^4}{\partial x^4} + 2(H_{12}^s + 2H_{66}^s)\frac{\partial^4}{\partial x^2 \partial y^2} + H_{22}^s\frac{\partial^4}{\partial y^4} - A_{44}^s\frac{\partial^2}{\partial y^2} - A_{55}^s\frac{\partial^2}{\partial x^2}.$$

4. Analytical solutions

For a plate simply supported on these four edges, *H*. Navier presented the external mechanical load as a double trigonometric series as

$q(x,y) = \sum_{m=1}^{+\infty}\sum_{n=1}^{+\infty} Q_{mn}\sin(\eta x)\sin(\mu y)$, where $\eta = \frac{m\pi}{a}$ et $\mu = \frac{n\pi}{b}$ and that $\forall\, m,n$ (16)

With: a is the width and b is the length of plate

• Case of a sinusoidal load $Q_{mn} = q_0$ for $m = n = 1$

• Case of a uniformly distributed load $Q_{mn} = \frac{16q_0}{\pi^2 mn}$ for $m = n = 1,3,5, \ldots$

And the same development for the travel field

$$\begin{cases} u_{x0}(x,y) &= \sum_{m=1}^{\infty}\sum_{n=1}^{\infty} U_x^{mn}.\cos(\eta x)\sin(\mu y) \\ u_{y0}(x,y) &= \sum_{m=1}^{\infty}\sum_{n=1}^{\infty} U_y^{mn}.\sin(\eta x)\cos(\mu y) \\ u_{z0}^{b}(x,y) &= \sum_{m=1}^{\infty}\sum_{n=1}^{\infty} U_{bz}^{mn}.\sin(\eta x)\sin(\mu y) \\ u_{z0}^{s}(x,y) &= \sum_{m=1}^{\infty}\sum_{n=1}^{\infty} U_{sz}^{mn}.\sin(\eta x)\sin(\mu y) \end{cases} \text{ and that } \forall\, m,n \tag{17}$$

Now we apply the operator matrix $[O]$ on the displacement vector $\{\delta\}$ of a point of the median plane we obtain another form of writing the system (15), $[R]\{d_{mn}\} = \{f_{mn}\}$

$$[R]\{d_{mn}\} = \{f\} \Longrightarrow \begin{bmatrix} R_{11} & R_{12} & R_{13} & R_{14} \\ R_{12} & R_{22} & R_{23} & R_{24} \\ R_{13} & R_{23} & R_{33} & R_{34} \\ R_{14} & R_{24} & R_{34} & R_{44} \end{bmatrix} \begin{Bmatrix} U_x^{mn} \\ U_y^{mn} \\ U_{bz}^{mn} \\ U_{sz}^{mn} \end{Bmatrix} = \begin{Bmatrix} 0 \\ 0 \\ Q_{mn} \\ Q_{mn} \end{Bmatrix} \tag{18}$$

With $R_{ij} = R_{ji}$ and:

$$\begin{aligned} R_{11} &= -(A_{11}\eta^2 + A_{66}\mu^2) \\ R_{12} &= -(A_{12} + A_{66})\eta\mu \\ R_{13} &= B_{11}\eta^3 + (B_{12} + 2B_{66})\eta\mu^2 \\ R_{14} &= B_{11}^s\eta^3 + (B_{12}^s + 2B_{66}^s)\eta\mu^2 \\ R_{22} &= -A_{66}\eta^2 - A_{22}\mu^2 \\ R_{23} &= B_{22}\mu^3 + (B_{12} + 2B_{66})\eta^2\mu \\ R_{24} &= B_{22}^s\mu^3 + (B_{12}^s + 2B_{66}^s)\eta^2\mu \\ R_{33} &= D_{11}\eta^4 + 2(D_{12} + 2D_{66})\eta^2\mu^2 + D_{22}\mu^4 \\ R_{34} &= D_{11}^s\eta^4 + 2(D_{12}^s + 2D_{66}^s)\eta^2\mu^2 + D_{22}^s\mu^4 \\ R_{44} &= H_{11}^s\eta^4 + 2(H_{12}^s + 2H_{66}^s)\eta^2\mu^2 + H_{22}^s\mu^4 + A_{44}^s\mu^2 + A_{55}^s\eta^2 \end{aligned}$$

The resolution of the system (18) allows us to obtain $d_{mn} = \{U_x^{mn}, U_y^{mn}, U_{bz}^{mn}, U_{sz}^{mn}\}^T$ and we go back to the displacement field (see (8)) and the following stress field (10)

$$\begin{Bmatrix} \sigma_x \\ \sigma_y \\ \tau_{xy} \end{Bmatrix}^{(k)} =$$

$$\sum_{m=1}^{\infty}\sum_{n=1}^{\infty}[Q]^{(k)} \begin{Bmatrix} [-\eta U_x^{mn} + z\eta^2 U_{bz}^{mn} + f(z)\eta^2 U_{sz}^{mn}]\sin(\eta x)\sin(\mu y) \\ [-\mu U_y^{mn} + z\mu^2 U_{bz}^{mn} + f(z)\mu^2 U_{sz}^{mn}]\sin(\eta x)\sin(\mu y) \\ [(\mu U_x^{mn} + \eta U_y^{mn}) - (2z\eta\mu U_{bz}^{mn} + 2f(z)\eta\mu U_{sz}^{mn})]\cos(\eta x)\cos(\mu y) \end{Bmatrix}^{(k)}.$$

$$\begin{Bmatrix} \tau_{yz} \\ \tau_{xz} \end{Bmatrix}^{(k)} = \sum_{m=1}^{\infty}\sum_{n=1}^{\infty} \begin{bmatrix} Q_{44} & 0 \\ 0 & Q_{55} \end{bmatrix}^{(k)} \begin{Bmatrix} \left(1 - \frac{\partial f}{\partial z}\right)\mu U_{sz}^{mn}\sin(\eta x)\cos(\mu y) \\ \left(1 - \frac{\partial f}{\partial z}\right)\eta U_{sz}^{mn}\cos(\eta x)\sin(\mu y) \end{Bmatrix}^{(k)} \tag{19}$$

These developments satisfy the conditions of the *k*-layer.

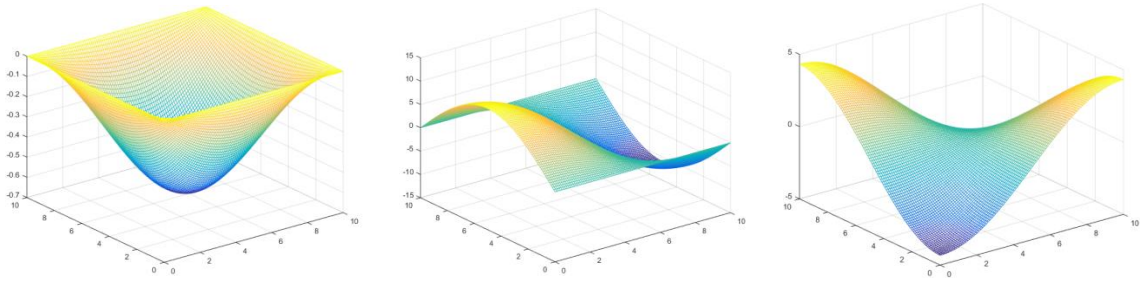

(a) Deflection $w(x,y,z)$ (b) Constraint $\tau_{xz}(x,y,z)$ (c) Constraint $\tau_{xy}(x,y,z)$

Fig. 3 Illustration of the maxima of the results for the $m = n = 1$

5. Numerical results and interpretations

5.1 Let's normalize the numerical results

The presentation of the numerical results is done in a non-dimensional way in order to normalize them and compare them with other results in the literature.

According to the simulations made with MATLAB for the displacement and stress fields we will use the following normalizations:

Non-dimensional thickness $\bar{z} = \frac{z}{h}$ Arrow: $\bar{u}_z = \frac{10h^3E}{a^4q_0}w(\frac{a}{2},\frac{b}{2})$

Shear stress $\bar{\tau}_{xy} = \frac{h}{aq_0}\tau_{xy}(0,b)$ Shear stress $\bar{\tau}_{xz} = \frac{h}{aq_0}\tau_{xz}(0,\frac{b}{2})$

Axial stress $\bar{\sigma}_x = \frac{h}{aq_0}\sigma_x(\frac{a}{2},\frac{b}{2},\frac{h}{2})$ Axial stress $\bar{\sigma}_y = \frac{h}{aq_0}\sigma_y(\frac{a}{2},\frac{b}{2},\frac{h}{2})$

5.2 Numerical results and discussion

• Global deflection and shear stress effects

The validation of the two models proposed in the present refined theory is done (after running the MATLAB program) by the models proposed by Arya *et al.* (2002), Karama *et al.* (2003), Reddy (2000).

The properties of the plate used in this comparative study are:

$\frac{a}{h} = 10$; $\frac{b}{a} = 1$; $a = 10$; Diagram [1-2-1]; $E_m = 70$ MPa; $E_c = 380$ MPa; $\nu = 0.3$

During this comparative survey of the overall deflection $\bar{u}_z$ and axial stresses $\bar{\sigma}_x$ and shear stresses $\bar{\tau}_{xz}$ of an FGM plate subjected under a sinusoidal load (SL) we observe a kind of agreement between the results of our models, 1 and 2, and the models cited in Reddy (2000), Zenkour (2009), Mantari *et al.* (2012). Same remarks regarding the reconciliation of the results found for a uniform load between the proposed models and the models in the literature.

The following part of the study aims to have the bending behavior of the FGM plate to target the variation of the aspect ratio a/h by applying the proposed model 1.

The properties of the plate used in this study are:

$\frac{b}{a} = 1$; Diagram [1-2-1]; $E_m = 70$ MPa; $E_c = 380$ MPa; $\nu = 0.3$

Table 3 Comparison of results for sinusoidal load (SL)

p	Results	Proposed model 1	Proposed model 2	Mantari *et al.* (2012)	Zenkour (2009)	Reddy (2000)
0		0.28448783	0.28153878	0.28322178	0.28355310	0.28289095
1	$\bar{u}_z$	0.50018398	0.49630778	0.49871718	0.49909829	0.49832686
10		0.88709997	0.88122531	0.88505559	0.88563658	0.88443569
0		1.96261115	1.98226349	1.97194643	1.96916321	1.97472575
1	$\bar{\sigma}_x$	0.80316840	0.81002481	0.80642534	0.80545432	0.80739501
10		1.13078748	1.14050164	1.13540192	1.13402617	1.13677573
0		0.15854168	0.15854168	0.15854168	0.15854168	0.15854168
1	$\bar{\tau}_{xy}$	1.03514073	1.03514073	1.03514073	1.03514073	1.03514073
10		355.462361	355.462361	355.462361	355.462361	355.462361
0		1.05679062	1.06737265	1.06181731	1.06031865	1.06331386
1	$\bar{\tau}_{xz}$	0.43247529	0.43616721	0.43422903	0.43370617	0.43475116
10		0.60888557	0.61411627	0.61137026	0.61062947	0.61211001

Table 4 The overall non-dimensional deflection $\bar{u}_z$ and the contribution of the deflection $\bar{u}_{z0}^s$ due to shear as a function of the ratio a/h

Load	p	Arrow	a/h				
			1	10	20	30	40
Sinusoidal load SL	0	$\bar{u}_z$	0.00000137	0.00671018	0.10638075	0.53763053	1.69815778
		$\bar{u}_{z0}^s$	0.00000222	0.00025419	0.00101789	0.00229073	0.00407270
		%	72.49 %	3.78 %	0.95 %	0.42 %	0.23 %
	1	$\bar{u}_z$	0.00000171	0.01175750	0.18740785	0.94808400	2.99567431
		$\bar{u}_{z0}^s$	0.00000200	0.00021867	0.00087530	0.00196967	0.00350179
		%	87.23 %	1.85 %	0.46 %	0.20 %	0.11 %
	10	$\bar{u}_z$	0.00000253	0.02082845	0.33266472	1.68356122	5.32027200
		$\bar{u}_{z0}^s$	0.00000190	0.00020382	0.00081573	0.00183558	0.00326338
		%	75.07 %	0.97 %	0.24 %	0.10 %	0.06 %
UL Uniform Load	0	$\bar{w}$	0.00000223	0.01087814	0.17245797	0.87157379	2.75294970
		$\bar{u}_{z0}^s$	0.00000359	0.00041208	0.00165015	0.00371360	0.00660242
		%	72.49 %	3.78 %	0.95 %	0.42 %	0.23 %
	1	$\bar{u}_{z0}^s$	0.00000278	0.01906055	0.30381416	1.53697589	4.85640427
		$\bar{w}^s$	0.00000325	0.00035450	0.00141898	0.00319311	0.00567690
		%	87.23 %	1.85 %	0.46 %	0.20 %	0.11 %
	10	$\bar{u}_z$	0.00000411	0.03376581	0.53929574	2.72928665	8.62490010
		$\bar{u}_{z0}^s$	0.00000308	0.00033043	0.00132242	0.00297574	0.00529039
		%	75.07 %	0.97 %	0.24 %	0.10 %	0.06 %

Table 4 summarizes the variation of the overall deflection $\bar{u}_z$ and the contribution of the shear deflection $\bar{u}_{z0}^s$ in terms of percentage, these results are presented in the curves of Fig. 4 (a), (b), (c).

A first analysis of these results indicates that the overall sag $\bar{u}_z$ (curves (a)) increases with the increase of the ratio a/h and this is correct because the plate will be thinner and thinner, but we

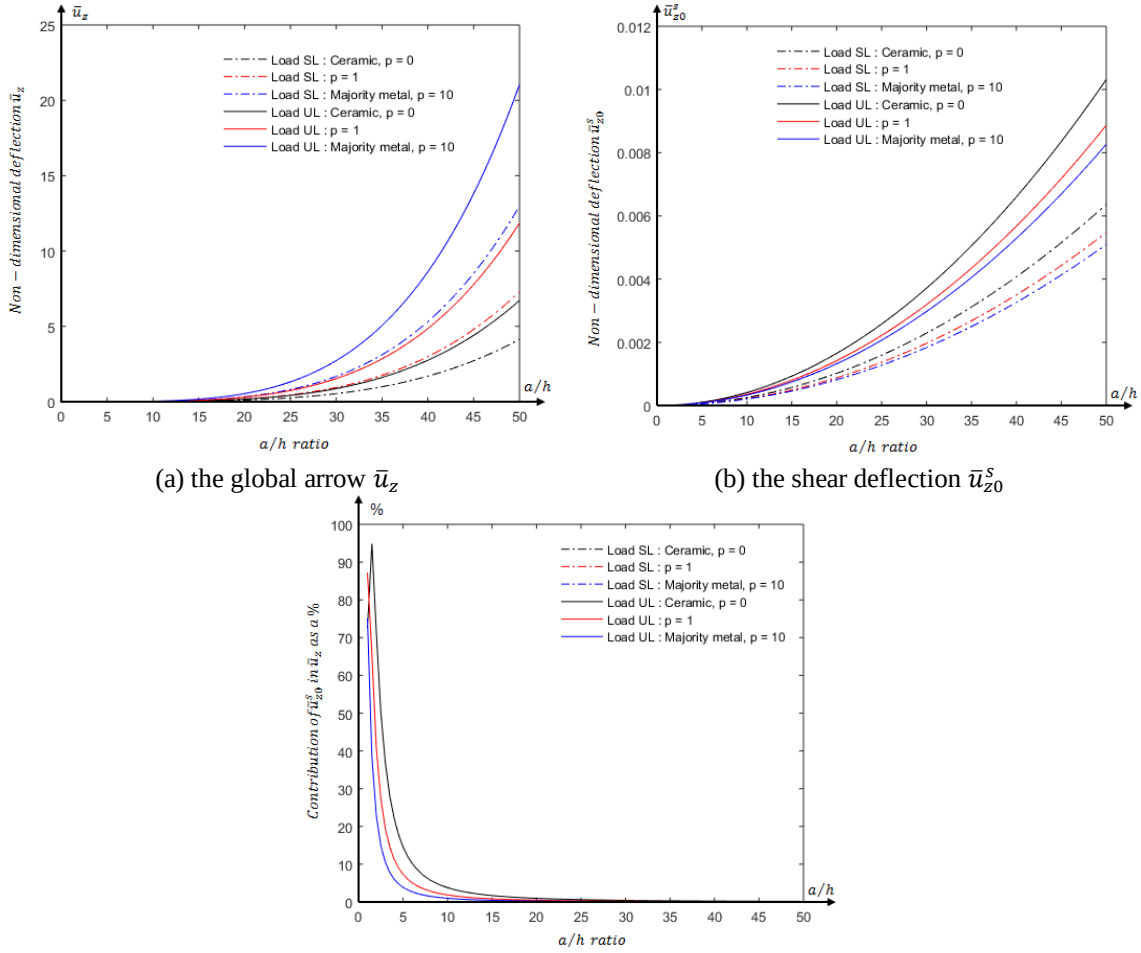

(a) the global arrow $\bar{u}_z$ (b) the shear deflection $\bar{u}^s_{z0}$

(c) the contribution as a percentage of $\bar{u}^s_{z0}$ in $\bar{u}_z$

Fig. 4 Illustration of the global deflections $\bar{u}_z$ and the contribution of the shear deflection $\bar{u}^s_{z0}$ in the deflection of the plate

observe a decrease in the contribution of the deflection due to shear $\bar{u}^s_{z0}$ (curves (c)) even it ($\bar{u}^s_{z0}$) also increases with the ratio a/h (curves (b)), so to explain this problem we say that for small ratios of a/h (thick plates) the global deflection $\bar{u}_z$ is very small while the shear effect will be very clear (87.23% the share of $\bar{u}^s_{z0}$ in $\bar{u}_z$) and the opposite will occur for large ratios a/h (0.23% share of $\bar{u}^s_{z0}$ in $\bar{u}_z$).

We observe an invariance of the contribution of the shear effect on the overall deflection even if we change the load of the FGM plate from uniform to sinusoidal.

We notice that the ceramic plate ($p = 0$) is less flexible under any load compared to the FGM plates (see curve a) while the shear stresses if we load the plate sinusoidally has a less important effect compared to the case of a uniform load.

Now we make a small tour on the effect of the shear stresses on the deflection of the FGM plate for the different scheme of the plate by applying the proposed model 1.

The properties of the plates used in this study are:

Table 5 The overall non-dimensional deflection $\bar{u}_z$ and the contribution of the deflection $\bar{u}_{z0}^s$ due to shear as a function of the layer scheme

Load	p	Arrow	Layering scheme				
			[1-1-1]	[1-2-1]	[2-1-2]	[1-1-3]	[1-1-0]
Sinusoidal load SL	0	$\bar{u}_z$	0.00671018	0.00671018	0.00671018	0.00671018	0.00671018
		$\bar{u}_{z0}^s$	0.00025419	0.00025419	0.00025419	0.00025419	0.00025419
		%	3.78 %	3.78 %	3.78 %	3.78 %	3.78 %
	1	$\bar{u}_z$	0.01368947	0.01175750	0.01517274	0.01289900	0.00876338
		$\bar{u}_{z0}^s$	0.00022539	0.00021867	0.00023863	0.00026304	0.00027270
		%	1.64 %	1.85 %	1.57 %	2.03 %	3.11 %
	10	$\bar{u}_z$	0.02800755	0.02082845	0.03258370	0.01985358	0.00854640
		$\bar{u}_{z0}^s$	0.00025649	0.00020382	0.00034484	0.00040519	0.00036076
		%	0.91 %	0.97 %	1.05 %	2.04 %	4.22 %

$$\frac{a}{h} = 10; \frac{b}{a} = 1; a = 10; E_m = 70 \text{ MPa}; E_c = 380 \text{ MPa}; \nu = 0.3$$

According to the general configuration [e-f-g] indicated in the note on page 3, the diagrams "[1-1-1]", "[1-2-1]", "[2-1-2]", "[1-0-1]" and "[1-1-3]" represent the ratios of the heights of the layers making up the FGM plate to the total height (the ratio of h_{Al} is e, of $h_{Al_2O_3}$ is f and of h_{Al} is g).

We notice that, even if we change the plate pattern, the global and shear deflection are always constant if $(p = 0)$ and this is because the plate is entirely made of ceramic.

The deflection increases significantly for the symmetrical schemes with the two extreme layers in FGM (layers 1 and 3) being larger ($\bar{u}_z = 0.01517274$) but the contribution of the shear stress effect is clearer for the non-symmetrical schemes 4.22 % for $(p = 10)$.

• Axial and transverse stresses

Let's study the behavior of the FGM plate at the axial and transverse stress level $\bar{\sigma}_x$ and transverse $\bar{\tau}_{xz}$ as a function of the applied power law, by applying the proposed model 1.

The properties of the plates used in this study are:

$$\frac{a}{h} = 10; \frac{b}{a} = 1; a = 10 \;\; E_m = 70 \text{ MPa}; E_c = 380 \text{ MPa}; \nu = 0.3$$

According to the general configuration [e-f-g] indicated in the note on page 3, the diagrams "[1-1-1]", "[1-2-1]", "[2-1-2]", "[1-0-1]" and "[1-1-3]" represent the ratios of the heights of the layers making up the FGM plate to the total height (the ratio of h_{Al} is e, of $h_{Al_2O_3}$ is f and of h_{Al} is g).

Table 6 shows the variation of stresses $\bar{\sigma}_x$ and $\bar{\tau}_{xz}$ for the different schemes as a function of the index $p \in \{0,0.5,1,10\}$ of a plate under sinusoidal and then uniform loading, the leafing of these results shows that, passing from the sinusoidal load SL to that uniform, both axial and transverse stresses increase, these results are drawn in Fig. 5.

According to the general configuration [e-f-g] indicated in the note on page 3, the diagram [1-2-1], [1-1-3] represents the ratios of the heights of the layers making up the FGM plate to the total height (the ratio of h_{Al} is 1, of $h_{Al_2O_3}$ is 1 and of h_{Al} is 3).

Of the four curves which differ by the material constitution according to the index $p \in \{0,0.5,1,10\}$ in the same figure and by the geometrical property (thickness of layers) between the two figures, we note the following results:

Table 6 Maximum axial stress $\bar{\sigma}_x$ and transverse $\bar{\tau}_{xz}$ as a function of the p-value for different schemes and loads

Result	Load	p	Scheme				
			[1-1-1]	[1-2-1]	[2-1-2]	[1-0-1]	[1-1-3]
Axial stress $\bar{\sigma}_x$	SL	0	1.96261115	1.96261115	1.96261115	1.96261115	1.96261115
		0.5	0.56510870	0.51608932	0.60102012	0.64830682	0.59913535
		1	0.74229495	0.63721200	0.82287924	0.93019657	0.77820059
		10	1.52089679	1.13078748	1.76977322	1.93232969	1.28606152
	UL	0	3.18166536	3.18166536	3.18166536	3.18166536	3.18166536
		0.5	0.91611972	0.83665250	0.97433712	1.05099543	0.97128165
		1	1.20336325	1.03300919	1.33400158	1.50797789	1.26157128
		10	2.46558502	1.83316362	2.86904828	3.13257490	2.08488442
Transverse stress $\bar{\tau}_{xz}$	SL	0	1.05679062	1.05679062	1.05679062	1.05679062	1.05679062
		0.5	0.30428930	0.27789425	0.32362622	0.34908828	0.32261134
		1	0.39969728	0.34311415	0.44308882	0.50087508	0.41903108
		10	0.81894443	0.60888557	0.95295481	1.04048521	0.69249466
	UL	0	1.71320442	1.71320442	1.71320442	1.71320442	1.71320442
		0.5	0.49329523	0.45050519	0.52464306	0.56592061	0.52299781
		1	0.64796483	0.55623571	0.71830854	0.81198809	0.67930761
		10	1.32762270	0.98708810	1.54487215	1.68677110	1.12263007

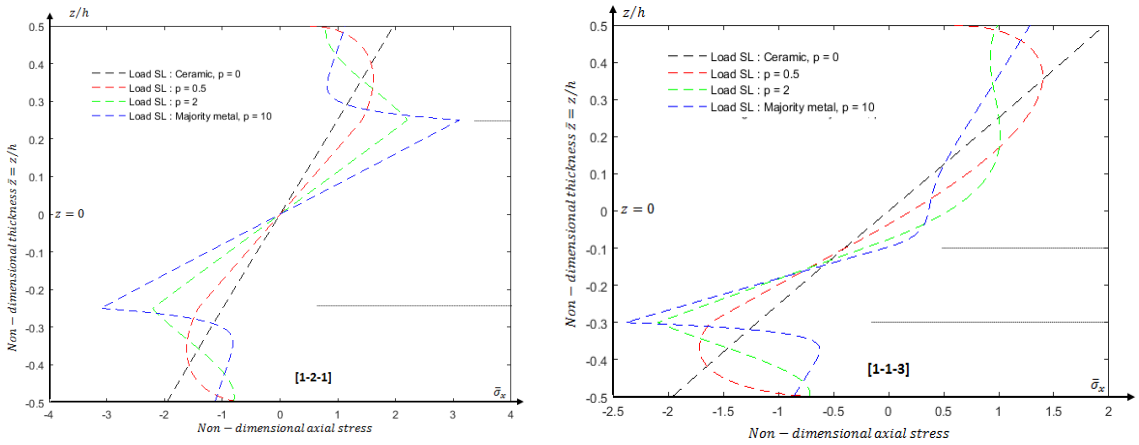

(a) Diagram [1-2-1] (b) Diagram [1-1-3]

Fig. 5 Variation of dimensionless axial stresses $\bar{\sigma}_x$ through the thickness

The axial stress is symmetrical with respect to the neutral plane in the case of symmetrical schemes, whereas in the case of non-symmetrical schemes the neutral plane changes geometry as well, so the stress distribution is not symmetrical.

In the case of symmetrical patterns the maximum axial stress occurs at the interface between the central layer (all-ceramic layer) and the 3$^{\text{ème}}$ FGM layer, fortunately the transition between the layers is not abrupt, so we do not have delamination problems.

According to the executions made under MATLAB we have obtained a special behavior of the

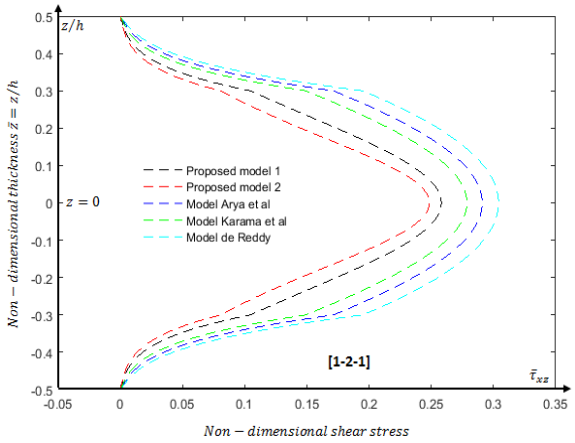

Fig. 6 Stress comparison $\bar{\tau}_{xz}$ for the different models

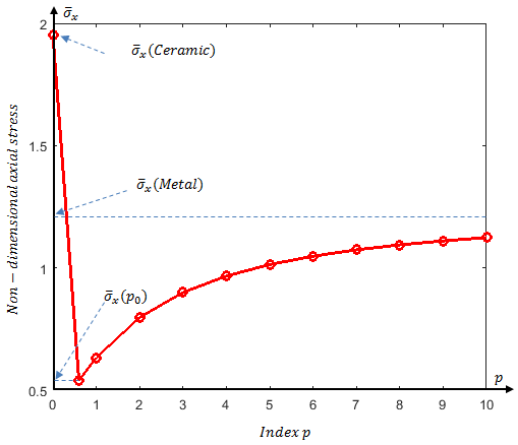

Fig. 7 Maximum axial stress a dimensional $\bar{\sigma}_x$ on the upper surface of the FGM plate

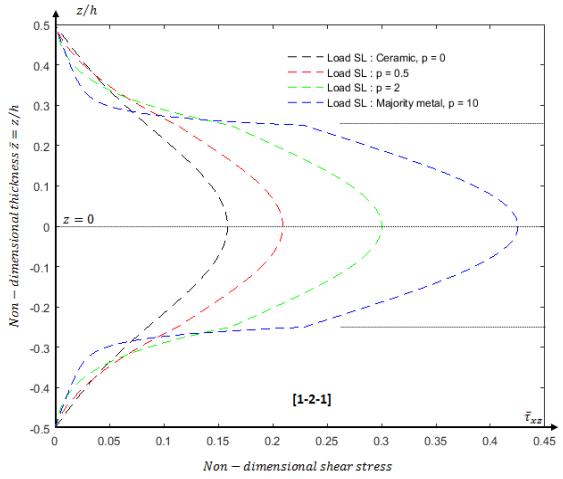

(a) Diagram [1-2-1]

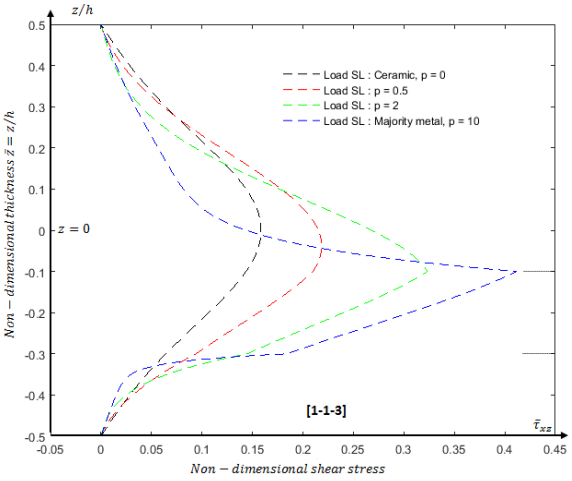

(b) Diagram [1-1-3]

Fig. 8 Variation of dimensionless transverse stresses $\bar{\tau}_{xz}$ through the thickness

axial stress on both the high and low faces of the FGM plate this stress $\bar{\sigma}_x$ is always between the maximum axial stress of a full ceramic plate $\bar{\sigma}_x(p = 0)$ and the stress of an FGM plate whose index p takes a particular value between 0 and 1, $\bar{\sigma}_x(p = p_0)$

In the case where $(p \neq 0)$ always the axial stress $\bar{\sigma}_x$ is between $\bar{\sigma}_x(p = p_0)$ and $\bar{\sigma}_x(p \to +\infty)$ this is the case of a metal plate, see Fig. 7.

After the graphical illustration of the maximum non-dimensional axial stress of an FGM plate for different values of the index p, this index has a significant effect on the axial stress supported by the FGM plate on the faces.

According to the general configuration [e-f-g] indicated in the note on page 3, the diagram [1-2-1], [1-1-3] represents the ratios of the heights of the layers making up the FGM plate to the total height (the ratio of h_{Al} is 1, of $h_{Al_2O_3}$ is 1 and of h_{Al} is 3).

According to the approximation made by the proposed shape function $f(z)$ (proposed model 1), the maximum non-dimensional shear stress through the plate thickness shows that the effect of these stresses becomes increasingly important as the index p increases, this effect is symmetrical for geometrically symmetrical plates and non-symmetrical in other cases.

The shear stress according to the proposed model 1, $f(z) = \frac{h}{\pi}\sin(\sin\frac{\pi}{h}z)$, has a weaker effect for shallow depths in the plate from both sides and becomes stronger at the transition between layers, see Fig. 8.

6. Conclusions

We have studied and determined the effect of shear stresses on the overall deflection of an FGM plate constructed of three layers of Al/Al_2O_3/Al and so forth as well as on the maximum axial stress on both sides of the plate, this study was based on the use of a refined theory with only four unknowns and a proposed shape function that satisfies a certain accuracy close to that given by very well-known models in the literature we concluded that the contribution of shear effects influences the deflection of the plate for small ratios a/h but they can be neglected for thin plates. Therefore, we can say that this study is correct whatever the adopted scheme. Also the use of the power law imposes the correct choice of their index p in order to respect the admissible axial stress on the top and bottom faces of the plate. The effect of shear stresses on plate deflection is clear for FGM plates and have a low contribution in deflection of all-ceramic plates.

References

Abdelbaki, B.M., Mohamed Sayed, M.E.A. and Al Kaisy, A.M. (2022), "A parametric study on the free vibration of a functionally graded material circular plate with non-uniform thickness resting on a variable pasternak foundation by differential quadrature method", *Couple. Syst. Mech.*, **11**(4), 357-371 https://doi.org/10.12989/csm.2022.11.4.357.

Aghababaei, R. and Reddy, J.N. (2009), "Nonlocal third-order shear deformation plate theory with application to bending and vibration of plates", *J. Sound Vib.*, **326**(1-2), 277-289. https://doi.org/10.1016/j.jsv.2009.04.044.

Arslan, K. and Gunes, R. (2018), "Experimental damage evaluation of honeycomb sandwich structures with Al/B_4C FGM face plates under high velocity impact loads", *Compos. Struct.*, **202**, 304-312. https://doi.org/10.1016/j.compstruct.2018.01.087.

Arya, H., Shimpi, R.P. and Naik, N.K. (2002), "A zigzag model for laminated composite beams", *Compos. Struct.*, **56**(1), 21-24. https://doi.org/10.1016/s0263-8223(01)00178-7.

Bai, E. and Chen, A. (2012), "A symplectic eigenfunction expansion approach for free vibration solutions of rectangular kirchhoff plates", *J. Vib. Control*, **19**(8), 1208-1215. https://doi.org/10.1177/1077546312448503.

Bekki, H., Benferhat, R. and Daouadji, T.H. (2021), "Vibration analysis of porous FGM plate resting on elastic foundations: Effect of the distribution shape of porosity", *Couple. Syst. Mech.*, **10**(1), 61-77. https://doi.org/10.12989/csm.2021.10.1.061.

Belkhodja, Y., Belkhodja, M.E., Fekirini, H. and Ouinas, D. (2023), "New quasi-three-, and two-dimensional trigonometric-cubic monomial HSDT for thermal buckling and thermo-mechanical bending analyses of FGM symmetrical/non-symmetrical sandwich plates with hard/soft core", *Compos. Struct.*, **304**, 116402. https://doi.org/10.1016/j.compstruct.2022.116402.

Benyoucef, S., Mechab, I., Tounsi, A., Fekrar, A., Ait Atmane, H. and Adda Bedia, E.A. (2010), "Bending of thick functionally graded plates resting on winkler-pasternak elastic foundations", *Mech. Compos. Mater.*, **46**(4), 425-434. https://doi.org/10.1007/s11029-010-9159-5.

Bhaskar, D.P., Thakur, A.G., Sayyad, I.I. and Bhaskar, S.V. (2021), "Numerical analysis of thick isotropic and transversely isotropic plates in bending using Fe based new inverse shear deformation theory", *Int. J. Auto. Mech. Eng.*, **18**(3), 8882-8894. https://doi.org/10.15282/ijame.18.3.2021.04.0681.

Bouhlali, M., Chikh, A., Bouremana, M., Kaci, A., Bourada, F., Belakhdar, K. and Tounsi, A. (2019), "Nonlinear thermoelastic analysis of FGM thick plates", *Couple. Syst. Mech.*, **8**(5), 439-457. https://doi.org/10.12989/csm.2019.8.5.439.

Fazzolari, F.A. and Carrera, E. (2014), "Coupled thermoelastic effect in free vibration analysis of anisotropic multilayered plates and FGM plates by using a variable-kinematics ritz formulation", *Eur. J. Mech.-A/Solid.*, **44**, 157-174. https://doi.org/10.1016/j.euromechsol.2013.10.011.

Garg, A., Belarbi, M.O., Chalak, H.D. and Chakrabarti, A. (2020). "A review of the analysis of sandwich FGM structures", *Compos. Struct.*, **258**, 113427. https://doi.org/10.1016/j.compstruct.2020.113427.

Javaheri, R. and Eslami, M.R. (2002), "Thermal buckling of functionally graded plates based on higher order theory", *J. Therm. Stress.*, **25**(7), 603-625. https://doi.org/10.1080/01495730290074333.

Jin, Z.H. and Batra, R.C. (1996), "Stresses intensity relaxation at the tip of an edge crack in a functionally graded material subjected to a thermal shock", *J. Therm. Stress.*, **19**, 317-339. https://doi.org/10.1080/01495739608946178.

Kablia, A., Benferhat, R. and Tahar, H.D. (2022), "Dynamic of behavior for imperfect FGM plates resting on elastic foundation containing various distribution rates of porosity: Analysis and modelling", *Couple. Syst. Mech.*, **11**(5), 389-409. https://doi.org/10.12989/csm.2022.11.5.389.

Karakoti, A., Pandey, S. and Kar, V.R. (2022), "Nonlinear transient analysis of porous P-FGM and S-FGM sandwich plates and shell panels under blast loading and thermal environment", *Thin Wall. Struct.*, **173**, 108985. https://doi.org/10.1016/j.tws.2022.108985.

Karama, M., Afaq, K.S. and Mistou, S. (2003), "Mechanical behaviour of laminated composite beam by the new multi-layered laminated composite structures model with transverse shear stress continuity", *Int. J. Solid. Struct.*, **40**(6), 1525-1546. https://doi.org/10.1016/s0020-7683(02)00647-9.

Kumar, Y. and Lal, R. (2012), "Vibrations of nonhomogeneous orthotropic rectangular plates with bilinear thickness variation resting on winkler foundation", *Meccanica*, **47**(4), 893-915. https://doi.org/10.1007/s11012-011-9459-4.

Liang, C. and Wang, Y.Q. (2020), "A quasi-3D trigonometric shear deformation theory for wave propagation analysis of FGM sandwich plates with porosities resting on viscoelastic foundation", *Compos. Struct.*, **247**, 112478. https://doi.org/10.1016/j.compstruct.2020.112478.

Liu, B.L., Li, S. and Li, Y.S. (2023), "Bending of FGM sandwich plates with tunable auxetic core using DQM", *Eur. J. Mech. A Solid.*, **97**, 104838. https://doi.org/10.1016/j.euromechsol.2022.104838.

Mahamood, R.M. and Akinlabi, E.T. (2017), *Functionally Graded Materials*, Springer International Publishing AG, 6330 Cham, Switzerland.

Mantari, J.L., Oktem, A.S. and Guedes Soares, C. (2012), "Bending response of functionally graded plates by using a new higher order shear deformation theory", *Compos. Struct.*, **94**(2), 714-723. https://doi.org/10.1016/j.compstruct.2011.09.007.

Mori, T. and Tanaka, K. (1973), "Average stress in matrix and average elastic energy of materials with misfitting inclusions", *Acta Metallurgica*, **21**(5), 571-574. https://doi.org/10.1016/0001-6160(73)90064-3

Najafizadeh, M.M. and Hedayati, B. (2004), "Refined theory for thermoelastic stability of functionally graded circular plates", *J. Therm. Stress.*, **27**(9), 857-880. https://doi.org/10.1080/01495730490486532.

Nguyen-Xuan, H., Tran, L.V., Nguyen-Thoi, T. and Vu-Do, H.C. (2011), "Analysis of functionally graded plates using an edge-based smoothed finite element method", *Compos. Struct.*, **93**(11), 3019-3039. https://doi.org/10.1016/j.compstruct.2011.04.028.

Nguyen-Xuan, H., Tran, L.V., Thai, C.H. and Nguyen-Thoi, T. (2012), "Analysis of functionally graded plates by an efficient finite element method with node-based strain smoothing", *Thin Wall. Struct.*, **54**, 1-18. https://doi.org/10.1016/j.tws.2012.01.013.

Rabboh, S.A. (2013). "The effect of functionally graded materials into the sandwich beam dynamic performance", *Mater. Sci. Appl.*, **4**(11), 751. https://doi.org/10.4236/msa.2013.411095.

Rao, M.K. and Desai, Y.M. (2004), "Analytical solutions for vibrations of laminated and sandwich plates using mixed theory", *Compos. Struct.*, **63**(3-4), 361-373. https://doi.org/10.1016/s0263-8223(03)00185-5.

Reddy, J.N. (1984), "A simple higher-order theory for laminated composite plates", *J. Appl. Mech.*, **51**(4), 745. https://doi.org/10.1115/1.3167719.

Reddy, J.N. (2000), "Analysis of functionally graded plates", *Int. J. Numer. Meth. Eng.*, **47**(1-3), 663-684. https://doi.org/10.1002/(sici)1097-0207(20000110/30)47:1/3<663::aid-nme787>3.0.co;2-8.

Rizov, V.I. (2021), "Delamination analysis of multi-layered beams exhibiting creep under torsion", *Couple. Syst. Mech.*, **10**(4), 317-331. https://doi.org/10.12989/csm.2021.10.4.317.

Sadeghi, Z. (2021), "Dynamic response analysis of a foam based nano scale plate based on finite strip method", *Couple. Syst. Mech.*, **10**(4) 281-298. https://doi.org/10.12989/csm.2021.10.4.281.

Sahoo, B., Sharma, N., Sahoo, B., Ramteke, P.M., Panda, S.K. and Mahmoud, S.R. (2022), "Nonlinear vibration analysis of FGM sandwich structure under thermal loadings", *Struct.*, **44**, 1392-1402. https://doi.org/10.1016/j.istruc.2022.08.081.

Singh, S.J. and Harsha, S.P. (2020). "Thermo-mechanical analysis of porous sandwich S-FGM plate for different boundary conditions using Galerkin Vlasov's method: A semi-analytical approach", *Thin Wall. Struct.*, **150**, 106668. https://doi.org/10.1016/j.tws.2020.106668.

Soelarso, S., Antaluca, E., Batoz, J.L. and Lamarque, F. (2021), "On the finite element modeling of a particular shallow foundation system for soft soil", *Couple. Syst. Mech.*, **10**(3), 247-261. https://doi.org/10.12989/csm.2021.10.3.247.

Swaminathan, K. and Patil, S.S. (2008), "Analytical solutions using a higher order refined computational model with 12 degrees of freedom for the free vibration analysis of antisymmetric angle-ply plates", *Compos. Struct.*, **82**(2), 209-216. https://doi.org/10.1016/j.compstruct.2007.01.001.

Taczala, M., Buczkowski, R. and Kleiber, M. (2022), "Analysis of FGM plates based on physical neutral surface using general third-order plate theory", *Compos. Struct.*, **301**, 116218. https://doi.org/10.1016/j.compstruct.2022.116218.

Thai, H.T. and Kim, S.E. (2012), "Levy-type solution for free vibration analysis of orthotropic plates based on two variable refined plate theory", *Appl. Math. Model.*, **36**(8), 3870-3882. https://doi.org/10.1016/j.apm.2011.11.003.

Youcef, A., Bourada, M., Draiche, K., Boucham, B., Bourada, F. and Addou, F.Y. (2020), "Bending behaviour of FGM plates via a simple quasi 3D and 2D shear deformation theories", *Couple. Syst. Mech.*, **9**(3), 237-264. https://doi.org/10.12989/csm.2020.9.3.237.

Zenkour, A.M. (2006), "Generalized shear deformation theory for bending analysis of functionally graded plates", *Appl. Math. Model.*, **30**(1), 67-84. https://doi.org/10.1016/j.apm.2005.03.009.

Zenkour, A.M. (2009), "The refined sinusoidal theory for FGM plates on elastic foundations", *Int. J. Mech. Sci.*, **51**(11-12), 869-880. https://doi.org/10.1016/j.ijmecsci.2009.09.026.

CC